

Momentum flux budget analysis of wind-driven air-water interfaces

Tobias Kukulka and Tetsu Hara

Graduate School of Oceanography, University of Rhode Island, Narragansett, Rhode Island, USA

Received 10 December 2004; revised 21 July 2005; accepted 13 October 2005; published 20 December 2005.

[1] Accurate knowledge of the air-sea momentum flux plays a critical role in ocean-atmosphere modeling. In this study we investigate the momentum flux budget at an air-water interface in the presence of wind-driven gravity-capillary waves. At the air-sea interface the total momentum flux (wind stress) partitions into viscous and wave-induced stress; the latter transfers momentum into surface waves. We estimate the wave growth rate (momentum transfer rate into waves) to close the momentum flux budget, using previous laboratory measurements of total and viscous stress, as well as surface wave spectra. The wave-induced stress is computed via a parameterized wave growth rate, which is proportional to the turbulent stress divided by the wave-phase speed squared. The constant of proportionality is then determined under two different assumptions. The first assumption (nonsheltering assumption) is that the turbulent stress is equal to the total wind stress. In the second assumption (sheltering assumption) the wave growth rate is determined by the local turbulent stress, which is a reduced turbulent stress due to the presence of longer waves. Both assumptions yield simple closed form expressions for the stress-partitioning ratio (ratio between the total stress and the viscous stress). With the sheltering assumption the growth rate agrees with previous theoretical and empirical estimates. Without sheltering, the growth rate is significantly lower than previous estimates. Therefore our results indicate that the growth rate of surface waves is determined by the local, reduced turbulent stress rather than the total wind stress.

Citation: Kukulka, T., and T. Hara (2005), Momentum flux budget analysis of wind-driven air-water interfaces, *J. Geophys. Res.*, 110, C12020, doi:10.1029/2004JC002844.

1. Introduction

[2] Accurate knowledge of the air-sea momentum flux is integral to ocean-atmosphere modeling. At the air-water interface the total momentum flux partitions into viscous stress and wave-induced stress. The wave-induced stress is mainly due to the pressure force acting on a sloping interface and transfers momentum into surface waves. The momentum flux from wind to a particular Fourier wave component is determined by the wave growth rate, β , defined as the momentum transfer rate from wind to waves per unit wave momentum. Therefore β represents a key quantity in the air-sea momentum flux budget analysis.

[3] *Plant* [1982] compiled observed growth rates from earlier studies and found that β normalized by the wave frequency is proportional to the total wind stress divided by the phase speed squared. The constant of proportionality, c_β , was determined by *Plant* [1982] with large uncertainties of $\pm 50\%$. Consequently, it is of great interest to the ocean-atmosphere wave modeling community to reduce these uncertainties.

[4] Recent analytical and numerical calculations (see review section 7.2 by *Belcher and Hunt* [1998]) predict the c_β consistently lower than *Plant's* estimate for surface

gravity waves. These calculations and *Plant's* parameterization do not explicitly include viscous effects; although for short surface waves viscous stresses might play a crucial role in the energy transfer from wind to waves [*Miles*, 1962]. *Harris et al.* [1996] concluded from a numerical modeling study that viscous effects are important in wave growth. By introducing a second-order turbulence closure that takes viscous effects into account, *Meirink and Makin* [2000] numerically simulated air flow over waves and showed that the wave growth rate depends on the Reynolds number, Re (defined by the ratio of friction velocity times wavelength to kinematic viscosity of air). Their model results are consistent with the analytical model from *van Gastel et al.* [1985], who solved the Orr-Sommerfeld equation to determine growth rates for gravity-capillary waves, using asymptotic methods.

[5] Another factor determining c_β is the wave sheltering: if longer waves “shelter” shorter waves, c_β needs to increase to support the same momentum flux into the waves. *Belcher and Hunt* [1993] showed with an analytic model for slowly moving waves that the dominant contribution to wave growth results from the undulating wave shape. The wave undulation induces an asymmetric pressure perturbation because of the Reynolds shear stress in a small layer above the surface (the “inner region”). Consequently, the wave growth rate depends on the turbulent

stress inside the inner layer, which is called the local turbulent stress [Makin *et al.*, 1995; Belcher, 1999; Makin and Kudryavtsev, 1999]. If the vertical extent of the stress induced by longer waves exceeds the inner region height of shorter waves, longer waves effectively reduce the turbulent stress that is felt by shorter waves and thereby the longer waves shelter shorter waves [Makin *et al.*, 1995].

[6] Previous measurements of the growth rate of short wind waves were made in controlled laboratory settings by observing the initial wave growth just after the onset of the wind. Larson and Wright [1975] measured growth rates using microwave backscatter for wind-driven gravity-capillary waves. Kawai [1979] found that initial wind-generated wavelets grew exponentially. More recently, Uz *et al.* [2003] measured growth rates of gravity-capillary waves in oblique directions relative to the wind. Overall, the observed growth rates are consistent with the growth rates determined by Meirink and Makin [2000].

[7] All these observational studies estimated the growth rate by focusing on the initial stage of the wave growth when the effects of the nonlinear wave interaction and wave breaking are negligible. In this study, we use the overall momentum flux budget to estimate the growth rate. One of the objectives of the paper is to investigate the sensitivity of the stress partitioning on the sheltering and nonsheltering assumptions. Our approach is possible because of the recent theoretical and observational advancement of the stress partitioning at the air-water interface. We derive simple analytical formulas for the ratio of viscous to total stress that depend only on the wave field and c_β . The experiment by Banner and Peirson [1998] provides measurements of the total stress, viscous stress and the wave field. With the experimental data we may estimate the coefficient c_β .

[8] Waves of all scales (not just peak waves) may contribute to the overall wave induced stress. Therefore it is important to integrate the contributions from the entire wave spectrum. Our approach is based on the assumption that linear theory can be applied to model the momentum flux from wind to each wave spectral component. Unlike the initial wavelets observed by Kawai [1979], the strongly wind-forced waves of the experiment by Banner and Peirson [1998] show nonlinear features, such as wave breaking, particularly in the peak region of the spectrum. Still, we believe that the linear theory can be applied provided that a significant fraction of the momentum flux is supported by shorter waves away from the spectral peak. Last, our approach is data driven, so that nonlinear effects could be implicitly modeled through the fitting parameter c_β (e.g., if breaking waves enhance the momentum flux, c_β must be elevated).

2. Stress Partitioning at the Air-Sea Interface

[9] We start with the assumption that the surface wave field is a linear superposition of sinusoidal wave components. For a continuous spectrum of waves the dimensional input rate of momentum to waves is defined by

$$\beta(k, \theta) = \frac{M(k, \theta)}{\rho_w \omega \Psi(k, \theta)} \quad (1)$$

where Ψ is the two dimensional wave number spectrum, ρ_w denotes the density of water, and ω is the frequency of a

wave component. The denominator is the spectral wave momentum density while the numerator, M , represents the spectral momentum flux density into the waves with wave number k and propagating in the direction θ relative to the wind. The vertical momentum flux into the waves along the wind direction can be expressed as

$$\tau_w = \int_0^\infty \int_{-\pi/2}^{\pi/2} M \cos \theta k d\theta dk = \rho_w \int_0^\infty \int_{-\pi/2}^{\pi/2} \beta \omega k \Psi \cos \theta d\theta dk. \quad (2)$$

In (2) we assume for simplicity that all the waves propagate in angles between $-\pi/2$ and $\pi/2$ relative to the wind direction. At the air-water interface the total momentum flux, τ_0 , partitions into a viscous stress, τ_ν , and wave induced stress, τ_w ,

$$\tau_0 = \tau_\nu + \tau_w. \quad (3)$$

2.1. Wave Growth Rate

[10] To calculate the wave-induced stress via (2), we set the growth rate to

$$\beta(k, \theta) = c_\beta \omega \frac{\tau_\beta}{\rho_w c^2} h_\beta(\theta), \quad (4)$$

where, c is the wave-phase speed, and $h_\beta(\theta) = \cos^2 \theta$ is the directionality of the wave growth rate. As discussed below, $\tau_\beta(k)$ denotes the turbulent stress that determines the wave growth of waves at k . This parameterization is consistent with laboratory and field data [Plant, 1982], numerical model results by Mastenbroek *et al.* [1996], and is also in agreement with theoretical estimates [e.g., Belcher and Hunt, 1993]. In addition, this form allows easy comparison among growth rates because it is often used in the literature [e.g., Belcher and Hunt, 1998; Makin and Kudryavtsev, 1999; Meirink and Makin, 2000; Uz *et al.*, 2002]. In this study we assume that c_β is a function of Re only and is constant for large Re , i.e., for gravity waves (see discussion below). Note that c_β is a ‘‘bulk parameter’’ that hides important wave growth mechanisms such as the effects due to the undulating shape of the wave, the nonzero velocity at the surface of the wave, and a variable surface roughness [Belcher and Hunt, 1993]. In addition, the value of c_β may depend on wave sheltering [Makin and Kudryavtsev, 1999]. Simple analytic formulas for the ratio of the viscous to total stress highlight the difference between sheltered and nonsheltered waves.

2.2. No Sheltering

[11] In Plant’s original formula the turbulent stress τ_β that determines the wave growth rate is assumed to be equal to the total stress. We refer to this parameterization as the ‘‘nonsheltered’’ growth rate, because longer waves do not ‘‘shelter’’ shorter waves by reducing the local turbulent stress. Then, substitution of (4) into (2) yields, with (3)

$$\frac{\tau_\nu}{\tau_0} = 1 - c_I, \quad (5)$$

where

$$c_I = \int_0^\infty \int_{-\pi/2}^{\pi/2} c_\beta k^3 \Psi h_\beta(\theta) \cos \theta d\theta dk. \quad (6)$$

2.3. Sheltering

[12] The key idea of sheltering is that the turbulent stress τ_β in (4) decreases in the presence of a spectrum of waves, because waves extract wind momentum and thereby reduce the turbulent stress in the wave boundary layer [Makin and Kudryavtsev, 1999]. Belcher and Hunt [1993] showed for slowly moving gravity waves that the growth rate depends on the turbulent stress in the inner layer. The height, L , of the inner layer is defined such that eddies in the inner region reach equilibrium before they are advected by the mean wind, while outside the inner region eddies are rapidly distorted. Consequently, L depends on the wave number, the turbulent stress, and the wind speed profile. Furthermore, the analysis by Belcher and Hunt suggests that the wave-induced stress associated with waves at k decays across the inner region. Therefore, if the vertical extent of the stress induced by longer waves exceeds the inner layer height of shorter waves, longer waves reduce the turbulent stress that is felt by shorter waves.

[13] Following Hara and Belcher [2002], we introduce the following three assumptions. First, the growth rate of waves at k is determined by the local turbulent stress $\tau'_i(k)$, i.e., $\tau_\beta(k) = \tau'_i(k)$, and that the local turbulent stress is equal to the turbulent stress evaluated at the inner layer height, i.e., $\tau'_i(k) = \tau_i(z = L(k))$. Alternatively, τ'_i might be represented by an average of $\tau_i(z)$ from the surface to $L(k)$ [Makin and Kudryavtsev, 1999]. The sensitivity of the results to different assumptions of the local turbulent stress will be discussed in section 4.4. Second, the stress induced by waves at k is constant in the inner layer and zero outside. This step function approximation may be appropriate considering that the wave-induced stress rapidly decreases with height (see, e.g., discussion by Makin et al. [1995]) and is negligible outside the inner layer according to the theory by Belcher and Hunt [1993]. Makin et al. [1995] furthermore showed that approximating the total wave-induced stress as a step function provides similar predictions for the drag coefficient as compared to the results obtained with more complex decay functions. The third assumption is that the inner layer height L scales as $L = \delta/k$, where δ is a constant coefficient. Makin and Kudryavtsev [1999] and Hara and Belcher [2004] estimate δ approximately to 0.1 and 0.05, respectively. With these assumptions, the total (integrated) wave-induced stress at a height z is expressed as

$$\tau_w(z) = \int_0^{\delta/z} \int_{-\pi/2}^{\pi/2} c_\beta \tau'_i(k') k'^3 h_\beta(\theta) \Psi \cos \theta d\theta dk'. \quad (7)$$

Inside the constant stress layer the turbulent stress is

$$\tau_i(z) = \tau_0 - \tau_w(z). \quad (8)$$

Therefore the local turbulent stress, $\tau'_i(k)$, can be expressed as

$$\tau'_i(k) = \tau_i(z = L) = \tau_0 - \int_0^k \int_{-\pi/2}^{\pi/2} c_\beta \tau'_i(k') k'^3 h_\beta(\theta) \Psi \cos \theta d\theta dk', \quad (9)$$

where the second term on the right-hand side represents the integrated waveform drag due to waves with wave numbers between 0 and k .

[14] Note that the inner layer height $L = \delta/k$ becomes equal to the viscous sublayer height $z_\nu \sim 5\nu/u_{*v}$, at $Re_\nu = 2\pi u_{*v}/k\nu \sim 30/\delta$, where ν is the kinematic viscosity of air, Re_ν is the Reynolds number defined in terms of the surface viscous friction velocity $u_{*v} = (\tau_0/\rho)^{1/2}$, and ρ is the density of air. Taking $\delta = 0.05$, for waves with $Re_\nu > 600$, turbulence in the inner layer should in principle play a role in the wave growth and therefore the sheltering effect is important. For very short gravity-capillary waves with $Re_\nu < 600$ the inner region is dynamically insignificant [van Gastel et al., 1985] and the sheltering effect is likely unimportant. In our analysis, however, such short waves contribute less than 13% to the overall momentum flux. Therefore, for simplicity we assume that (9) is valid for the entire wave number range.

[15] Equation (9) can be differentiated with respect to k to obtain

$$\frac{d\tau'_i}{dk} = -c_\beta \tau'_i k^3 \int_{-\pi/2}^{\pi/2} h_\beta(\theta) \Psi \cos \theta d\theta. \quad (10)$$

With the boundary condition $\tau'_i(k = 0) = \tau_0$ and noting that $\tau'_i(k = \infty) = \tau_\nu$, integration of (10) results in

$$\frac{\tau_\nu}{\tau_0} = \exp(-c_I). \quad (11)$$

[16] Equations (5) and (11) compactly summarize the partitioning of viscous and wave-induced stress under the nonsheltering and sheltering assumptions. For $\Psi \rightarrow 0$ the total stress equals the viscous stress; that is, the flow is aerodynamically smooth. Note that the wave-induced stress can never exceed the total stress under the sheltering assumption, so that Plant's [1982] discussion of a limiting mean square slope in the wind direction becomes obsolete, on the basis of momentum constraints. For given viscous and total stress, the value of c_β will depend on the sheltering effect.

2.4. Viscous Effects on the Growth Rate

[17] Although c_β is assumed to be constant for gravity waves, the investigation by Meirink and Makin [2000] indicates that c_β depends on the Reynolds number, Re ($Re = 2\pi u_{*v}/k\nu$, where $u_{*v} = (\tau_0/\rho)^{1/2}$ is the air friction velocity). The numerical model of Meirink and Makin was set up for linear (small slope) monochromatic waves, for which the sheltering effect is negligible. Therefore the forcing stress τ_β in (4) was equated with the total wind stress.

[18] If the value of c_β is to be determined from (5) and (11) for gravity-capillary waves, the parameterization (4) should also explicitly depend on Re . In our approach we cannot directly use the c_β determined by Meirink and Makin [2000], since we attempt to estimate the c_β that best closes the momentum flux budget for the experiment by Banner and Peirson [1998]. Therefore we need to introduce a new parameterization that on one hand reflects the Reynolds number dependence found by Meirink and Makin [2000] and on the other hand has a free parameter that can be adjusted to best close the momentum flux budget.

Table 1. Summary of Stress Measurements by *Banner and Peirson* [1998]

Experiment Number	1	2	3	4	5	6
fetch, m	4.35	2.45	3.10	4.35	2.45	4.35
u_* , m/s	0.26	0.32	0.35	0.37	0.40	0.46
τ_0 , Pa	0.083	0.125	0.150	0.168	0.199	0.261
τ_v , Pa	0.052	0.074	0.073	0.074	0.088	0.082

[19] The new parameterization should satisfy the following two conditions. First, c_β is independent of Re for $Re > 10^4$ because viscous effects are negligible in this regime. Second, the value for c_β peaks at $Re \approx 800$, since the combination of viscous and turbulent stresses causes an enhanced pressure asymmetry, leading to maximal growth rates. One convenient way of representing these two properties, is to model the Re dependence of c_β as a piecewise linear function of $\ln(Re)$, peaking at $Re = 800$ and being constant at $c_{\beta\infty}$ for $Re > 10^4$,

$$\frac{c_\beta(Re)}{c_{\beta\infty}} = \begin{cases} 2 \frac{\ln(Re) - \ln(100)}{\ln(800) - \ln(100)} + 1 & \text{if } 100 < Re \leq 800 \\ 2 \frac{\ln(10^4) - \ln(Re)}{\ln(10^4) - \ln(800)} + 1 & \text{if } 800 < Re < 10^4 \\ 1 & \text{otherwise.} \end{cases} \quad (12)$$

On the basis of the study by *Meirink and Makin* [2000], we set $c_{\beta\max} = 3c_{\beta\infty}$ and $c_\beta \approx c_{\beta\infty}$ at $Re = 100$. Furthermore, we extrapolate c_β for $Re < 100$ by keeping the coefficient constant. This extrapolation is not critical, since in our study short waves with $Re < 100$ contribute less than 1% to the overall air-water momentum flux. The sensitivity of our results to a different Reynolds number dependence will be discussed in section 4.3. With the parameterization (12), we will estimate the constant coefficient $c_{\beta\infty}$ using experimental data by *Banner and Peirson* [1998]. Spectral peaks of the experiment by *Banner and Peirson* [1998] were in the range of $Re \approx 1500$ to 6000. Therefore it is indeed important to account for the Reynolds number effect.

3. Estimates of Total Stress, Viscous Stress, and Wave Spectrum

[20] In order to determine c_β via (5) or (11) and (12) we need the estimates of viscous stress, total stress, and wave spectrum. *Banner and Peirson* [1998] developed a particle image velocimetry technique that allowed laboratory measurements of velocity shear within the viscous sublayer ($< 200 \mu\text{m}$) of the instantaneous wind-driven air-water interface. Viscous stress measurements were obtained at fetches of 0.13, 2.45, 3.10, and 4.35 m under varying wind conditions (see Table 1). The dominant wind-generated waves had wavelengths ranging from 78 to 174 mm and more than half the dominant waves were breaking.

[21] The technique did not allow the determination of viscous stresses in wave troughs and in the spilling regions of breaking waves. Phase-averaged mean values for viscous stresses were estimated from the measured tangential stress distributions. Where tangential stresses could not be measured they were calculated by setting the tangential stress to zero at the toe of the spilling region and in the separated

airflow zone immediately downwind of it. Error estimates were based on the standard error of the mean, which was ± 0.01 Pa (less than 20%) for the viscous stress estimate and 20% for the total stress.

[22] The full two-dimensional wave number spectra are estimated from the combination of one-point wave height measurements and an empirical parametric model. As explained in Appendix A, we define the low-wave number spectrum for waves with $k < 200 \text{ rad m}^{-1}$ and the high wave number spectrum for $k > 200 \text{ rad m}^{-1}$. In order to obtain the low-wave number part of the spectrum, we first determine the frequency spectrum, which is calculated from the time series of wave height measurements. The frequency spectrum is then converted to the omnidirectional wave number spectrum, based on the dispersion relation for linear surface waves. At higher wave numbers the frequency spectrum is contaminated by Doppler shifted frequencies. Therefore we estimate the high-wave number part of the spectrum with a parametric model, based on previous observations of high-wave number spectra. The directional spreading is modeled with the parametric model from *Donelan et al.* [1985]. Details are discussed in Appendix A.

4. Results

4.1. Estimated Value of c_β

[23] The coefficient $c_{\beta\infty}$ is determined from the wave spectrum and the set of experimentally determined viscous and total stress measurements via a least squares fit from (5) or (11) and (12). With the sheltering assumption $c_{\beta\infty}$ is 9.4 ($c_{\beta\max} = 28.2$), while without sheltering $c_{\beta\infty}$ is 6.7 ($c_{\beta\max} = 20.1$). Our model results of the viscous stress are compared with the measurements in Figure 1 with these two selected values of $c_{\beta\infty}$. Naturally, the predicted viscous stresses under the sheltering assumption agree with the observations with $c_\beta = 9.4$ (left panel), while the predictions without sheltering agree with the measured viscous stresses with $c_\beta = 6.7$ (right panel). An important point here is that our predictions with both assumptions may reproduce the observations quite well (they agree within the error bars), but that the values of c_β are significantly different.

[24] As c_β increases, the wave-induced momentum flux is enhanced, so that the modeled viscous stress must decrease. Modeled viscous stresses are larger under the sheltering assumption, because the momentum transfer from wind to waves is less efficient for sheltered waves than for non-sheltered waves. The difference between the sheltered and nonsheltered waves is especially pronounced for the experiments with greater total stress. For greater c_β , the viscous stresses can be significantly underestimated under the non-sheltering assumption. In fact, as c_β increases, the modeled viscous stress may reach an unphysical negative value in the nonsheltering case, while the modeled viscous stress is bound between 0 and τ_0 in the sheltered case.

4.2. Error Analysis of c_β

[25] In order to estimate the error of our c_β , we calculate $c_{\beta i}$ for the i th experiment (Table 1) and take the standard deviation of the set of $c_{\beta i}$. This procedure results in a relative error of about 20%, which corresponds approximately to the 90% confidence intervals as determined from the linear regression analysis (assuming the stress ratio is

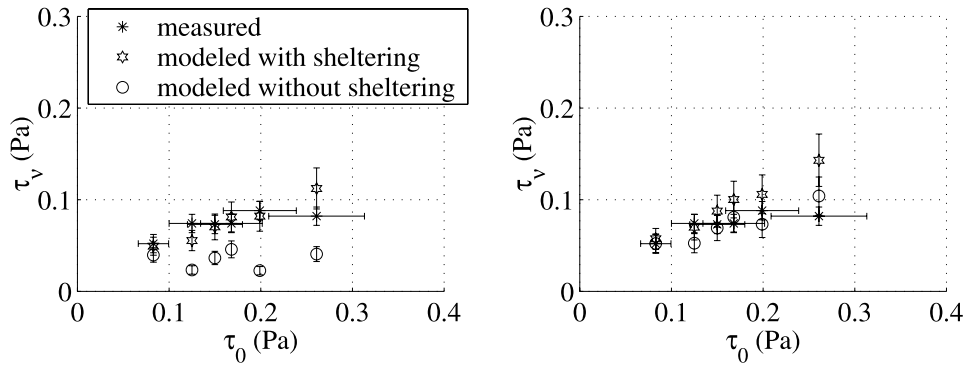


Figure 1. Comparison of modeled versus measured viscous stresses for two different $c_{\beta\infty}$ (measured (asterisks), modeled with (11) under the sheltering assumption (stars), and modeled with (5) without sheltering (circles)): (left) $c_{\beta\infty} = 9.4$ and (right) $c_{\beta\infty} = 6.7$. The errors of the measurements are based on estimates by *Banner and Peirson* [1998]; the model errors are determined by the errors of the measured total stress, which is the dominant source of error.

normally distributed and the wave spectrum given). The difference between the c_{β} determined for the sheltering and nonsheltering cases is significant, especially considering that the errors of both cases are correlated. This error estimate exceeds errors in c_{β} that are due to the uncertainties of the stress measurements or uncertainties of the wave spectrum. Gaussian error propagation of the error in the stress measurements results in a relative error of c_{β} below 13%. The uncertainty of the wave spectrum is mainly due to the parameterization at high wave numbers and the directional spreading. A 50% error in the omnidirectional short-wave spectrum causes a relative error of <11%. Assuming the extreme situation of a uniform directional spreading for

waves with $k > 150 \text{ rad m}^{-1}$, changes c_{β} at most by 9%. The variation of the parameter that determines the width of the directional spreading function causes a small relative error of less than 2% (b was varied between 0.7 and 1.7 for $k > 200 \text{ rad m}^{-1}$, see (A5) in Appendix A).

4.3. Comparison to Previous Estimates

[26] Figure 2 shows our results of c_{β} with the two (sheltering and nonsheltering) assumptions against the Reynolds number. Our c_{β} is generally smaller than the c_{β} determined by *Meirink and Makin* [2000]. Under the sheltering assumption, our results agree within two standard deviations with their numerical modeling results. For Re

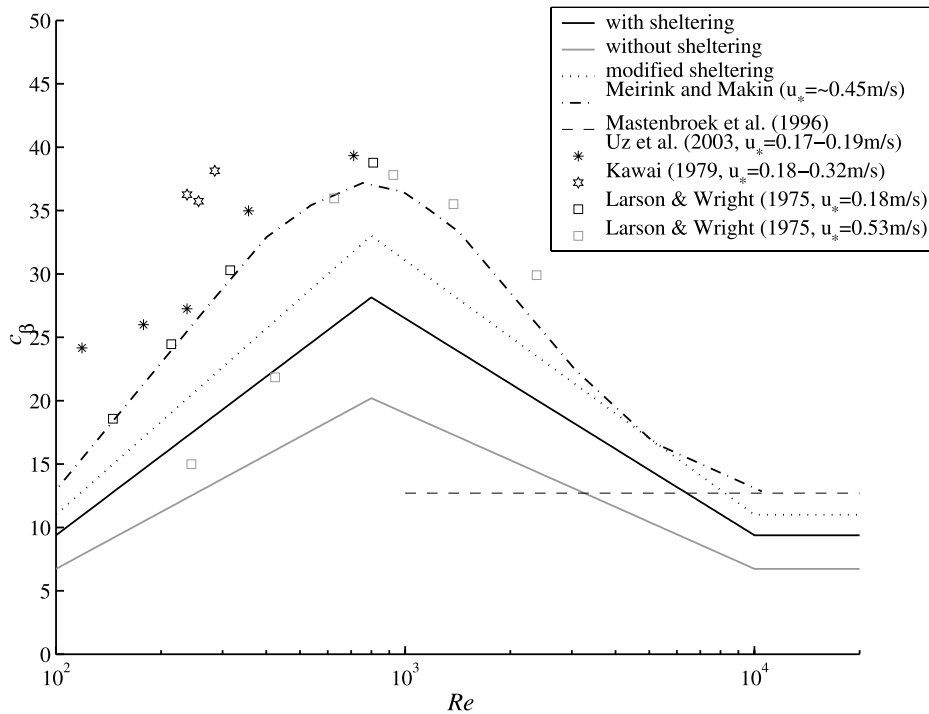


Figure 2. Comparison of our results for c_{β} with previous estimates. Modeling results by *Meirink and Makin* [2000] are roughly independent of u_* , for $u_* = 0.14$ to 0.9 m/s , and only the result of $u_* = 0.45 \text{ m/s}$ is shown.

close to the spectral peak ($Re \approx 1500$ to 6000), c_β is consistent with the lower limit of *Plant's* [1982] estimate of $c_\beta = 32 \pm 16$. Without sheltering, the estimates for c_β are significantly lower than the c_β determined by *Meirink and Makin* [2000] or *Plant* [1982]. The measured growth rates from *Uz et al.* [2003] agree reasonably well with model results from *Meirink and Makin* [2000]. Unfortunately, a direct comparison with the growth rates obtained by *Larson and Wright* [1975] and *Kawai* [1979] is ambiguous. *Larson and Wright* [1975] reported total surface stresses only after the wave field reached equilibrium. *Kawai* [1979] reported viscous stresses; however, *Banner and Peirson* [1998] point out the methodological problems in the measurements. Yet, for the sake of completeness we also include the measurements from *Kawai* and *Larson and Wright* (stresses were corrected after *Meirink and Makin*) in Figure 2. Then their results are also consistent with the c_β from *Meirink and Makin* [2000], except for a few cases.

[27] These comparisons clearly indicate that the sheltering effect is real and important, even for laboratory wind waves, since without sheltering our estimated value of c_β is significantly lower than all previous results.

[28] *Makin and Kudryavtsev* [1999] calculated the ratio of wave-induced to total stress for a fully developed sea and found reasonable agreement with the ratios from *Banner and Peirson's* experiment. However, the wave spectrum for a fully developed sea differs drastically from the short-fetch wave fields of *Banner and Peirson's* experiment. According to (5) or (11), the stress ratios could agree nevertheless if the coefficients c_l coincided for different wave spectra.

[29] Even for sheltered waves, our c_β appears to be underestimated. Note also that breaking waves likely increase the total stress because of the enhanced surface drag because of air flow separation [*Banner*, 1990]. In our approach this enhanced drag has not been considered separately. If the effects of breaking waves are to generate additional form drag without modifying the form drag of nonbreaking waves, as in the study by *Kudryavtsev and Makin* [2000], the value of c_β estimated here must decrease further.

[30] With hindsight, we can examine our assumption that a significant fraction of the momentum flux is supported by shorter waves away from the frequently breaking dominant wave. By first estimating the low-wave number part of the spectrum that contains longer breaking waves, we calculated how much of the wave-induced stress is supported by the remaining shorter waves (see Appendix B for details of this calculation). We find that these shorter waves contribute between 50% to 95%, on average about 65%, to the wave-induced stress. Therefore a significant fraction of the momentum flux is indeed supported by shorter waves.

[31] Our c_β might be underestimated because of the following reasons. First, we might have underestimated the total surface stress. Although the experiment by *Banner and Peirson* [1998] was designed to avoid pressure gradients, a horizontal pressure gradient would cause a height varying total stress that is largest at the surface. Secondly, the effects of sidewalls might decrease the wave growth rate for waves that propagate with an angle to the wind direction, because of the reduced wind stress close to the wall

(see discussion by *Uz et al.* [2003]). Thirdly, the Re dependence of c_β might differ from model (12). It is important to investigate the sensitivity of our results on different Reynolds number dependence parameterizations. As an extreme example, we have examined a case when c_β is assumed to be independent of Re (i.e., viscous effects are totally neglected). The value of c_β amounts to 19.7 and 13.5, for sheltered and nonsheltered waves, respectively. In this case, the value of c_β increases at high Reynolds numbers but decreases at Reynolds number around 800. Fourthly, the sheltering effect might be greater than represented here. The sheltering effect has been modeled in the spectral domain based on the assumption that all wave components are forced by the wind and propagate independently of other scales. However, parasitic capillary waves are usually located ahead of the wave crest, so that they might be sheltered differently from waves at the same wave number that are directly forced by winds. The sheltering effect is also greater than represented by (11) if the turbulent stress τ_β in (4) is smaller than the local turbulent stress τ'_l at the height of the inner layer. This possibility is examined next.

4.4. Enhanced Sheltering Effect

[32] With our sheltering assumption the turbulent stress that governs the wave growth of a wave component is the local turbulent stress, i.e., the turbulent stress in the inner region [*Belcher and Hunt*, 1993]. For simplicity, we have assumed that this local turbulent stress can be taken as the turbulent stress evaluated at the height of the inner region. The turbulent stress, however, decreases toward the surface. Therefore it is plausible that the local turbulent stress is given by the average turbulent stress in the inner region, i.e. $\tau_\beta(k) = \tau'_l(k) = L^{-1} \int_0^{L(k)} \tau_l(z) dz$ [see also *Makin and Kudryavtsev*, 1999]. To further simplify the algebra, we approximate this average by the mean of the viscous stress (i.e., the turbulent stress just outside the viscous sublayer), τ_ν , and the turbulent stress τ_l at height L ,

$$\tau_\beta = \frac{\tau_l(z=L) + \tau_\nu}{2}. \quad (13)$$

Following similar steps as discussed above leads to the differential equation

$$\frac{d\tau'_l}{dk} + c_\Psi \tau'_l = -c_\Psi \tau_\nu, \quad (14)$$

where

$$c_\Psi(k) = \frac{c_\beta k^3}{2} \int_{-\pi/2}^{\pi/2} \Psi h_\beta(\theta) \cos \theta d\theta. \quad (15)$$

The analytic solution is given by

$$\frac{\tau_\nu}{\tau_0} = \frac{1}{I(\infty) + \int_0^\infty c_\Psi I dk} \quad (16)$$

with the integrating factor $I(k) = \exp(\int_0^k c_\Psi dk')$. The c_β determined with enhanced sheltering effect agrees better with the modeling results from *Meirink and Makin* [2000] (see Figure 2). Note that the c_β for high Re also matches

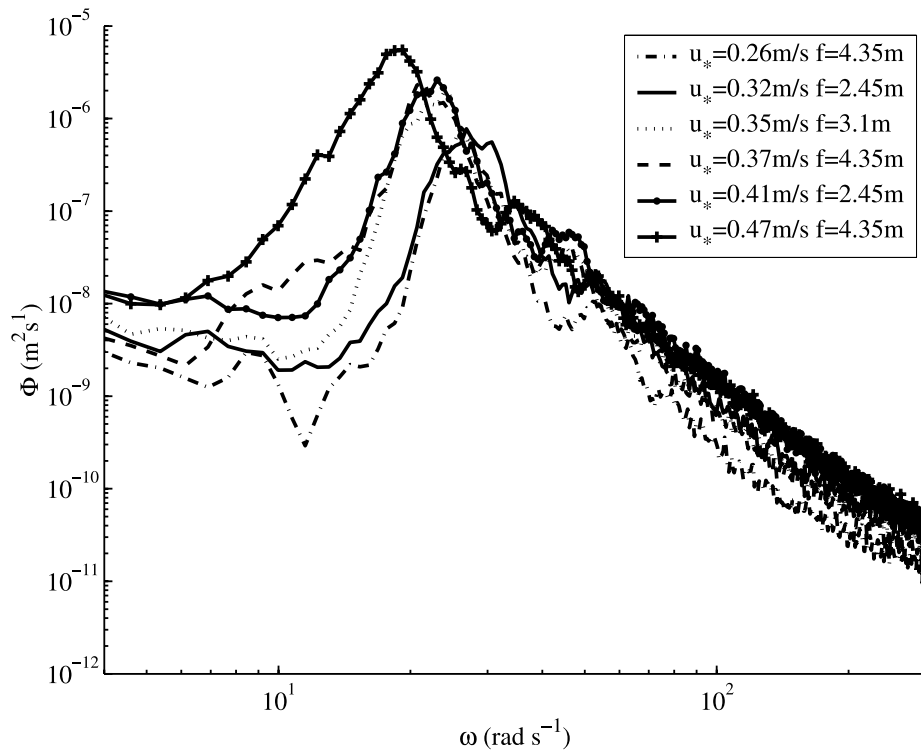


Figure A1. Frequency spectra calculated from wave height measurements (f : fetch).

well with the modeling results for high- Re flow by *Mastenbroek et al.* [1996].

5. Conclusions

[33] We have investigated the stress partitioning of the total stress into wave-induced and viscous components at an air-water interface in the presence of wind-driven gravity-capillary waves. Simple analytic formulas for the ratio of viscous to total stress have been derived under the sheltering and nonsheltering assumptions. In the sheltered case, it is assumed that the wave-induced stress of longer waves penetrates farther into the wave boundary layer than the wave-induced stress of shorter waves, thereby reducing the turbulent stress felt by shorter waves. The wave-induced stress was calculated from the wave growth rate, which is proportional to the turbulent stress divided by the wave-phase speed squared. The constant of proportionality, c_β , was then determined using the viscous and total stress measurements by *Banner and Peirson* [1998]. The value of c_β determined here is close to *Meirink and Makin's* [2000] numerically determined values and previous measurements under the sheltering hypothesis. Without sheltering, c_β is significantly lower than previous estimates. Thus our results indicate that the wave growth rate depends on the local reduced turbulent stress rather than the total stress.

[34] As shown earlier by *Meirink and Makin* [2000] the observed initial wave growth rate agrees reasonably well with theoretical predictions for lower Reynolds number range (less than a few thousands). Our results (with sheltering effect included) further show that the growth rates of the spectrum of waves is also consistent with the theory and observations for a similar Reynolds number range. At very high Reynolds numbers, however, the theoretical estimates

of the wave growth rate ($c_\beta \approx 15$) as well as our new estimates are less than half of observed growth rates (see discussion by *Belcher and Hunt* [1998]). This discrepancy remains one of the outstanding questions regarding the wind wave growth rate.

[35] Finally, if a significant fraction of smaller waves were breaking, airflow separation could disrupt the inner layer of longer waves. Then, the theory of smooth airflow over waves, on which our approach is based, would need to be modified to take the airflow separation effects into account. This will be a subject of our future investigation.

Appendix A: Wave Spectrum

[36] The omnidirectional wave spectrum is independently determined for long and short waves. The directionality of the wave number spectrum is estimated from an empirical parameter model.

A1. Long-Wave Spectrum

[37] The wave frequency spectrum was calculated from wave height measurements made at a sampling frequency of 1000 Hz and a record length of about 360s (Figure A1). Since the mean squared height is conserved, the frequency spectrum of linear surface waves can be converted to the omnidirectional wave number spectrum $\hat{\Psi}$ through

$$\hat{\Psi}(k) = \Phi(\omega)c_g \quad (\text{A1})$$

where $c_g = \partial\omega/\partial k$ is the group velocity. Simultaneous measurements of $\hat{\Psi}$ and Φ by *Hara et al.* [1997] confirm the approximate validity of (A1) at low wave numbers. Doppler shifted frequencies displace the observed spectral energy to higher-frequency waves [see, e.g., *Plant and Wright*, 1980]. Furthermore, the conversion (A1) is only valid for linear

Table A1. Least Squares Fit Results for the Coefficients in (A2)

	α	m	n	$\alpha(m=1, n=-2.8)$
Hara (fetch 13 m)	1.7×10^{-3}	0.36	-2.80	3.24×10^{-3}
Zhang (fetch 24 m)	2.2×10^{-3}	1.09	-2.69	3.25×10^{-3}
Jähne (fetch 100 m)	48.3×10^{-3}	1.41	-3.01	9.86×10^{-3}

surface waves. Steep short gravity-capillary waves, however, may transfer energy nonlinearly to capillary waves ahead of the crest [Longuet-Higgins, 1963]. Considering in addition the likely contamination of the high-frequency wave signal due to the intrusive measurement of the impedance wire probe, it is sensible to parameterize the wave number spectrum for high wave numbers.

A2. Short-Wave Spectrum

[38] The fetch dependency of the high-wave number spectrum can be investigated with measured wave number spectra of gravity-capillary waves by Jähne and Riemer [1990], Zhang [1995], and Hara *et al.* [1997] at fetches of 100 m, 24 m, and 13 m, respectively. A simple model of

$$\hat{\Psi}(k) = \alpha u_*^m k^n \quad (\text{A2})$$

is used in this study, where the coefficients α (in IS units), m , and n are first independently calculated for wave data from each study (see Table A1). On the basis of the results of this first iteration, we then set $n = -2.8$ and $m = 1$ and determine α as a function of fetch. This second iteration indicates that α increases with fetch, although the increase

is ambiguous for the shorter fetch cases. The value of α is influenced by the nonlinear energy transfer from short gravity waves to parasitic gravity-capillary waves [Longuet-Higgins, 1963; Kudryavtsev *et al.*, 1999], which might be relatively large at shorter fetches because of the relatively small peak wavelength. In light of these uncertainties, we set α to 3×10^{-3} for any fetch smaller than 5 m and assume a generous relative error of $\pm 50\%$. A comparison of measured and parameterized high-wave number spectra is shown in Figure A2. Our values of m and n are in agreement with Jähne and Riemer's finding that $\hat{\Psi}$ is proportional to $k^{-2.5}$ and u_* for small gravity waves under high wind speeds. The wave number dependency is also consistent with Elfouhaily *et al.*'s [1997] short-wave number parameter form, which also converges to $\hat{\Psi} \propto k^{-2.5}$ for capillary waves. The short omnidirectional wave number spectrum from Kudryavtsev *et al.* [1999] is in close agreement with the measurements by Hara *et al.* [1997] and thus consistent with our omnidirectional spectrum estimate. The reason why we did not use the short-wave spectrum by Elfouhaily *et al.* is that their corresponding α value is fetch-independent and matches best the long-fetch data from Jähne and Riemer. Following Elfouhaily *et al.* [1997], we model viscous damping of very short waves by multiplying the high-wave number spectrum by the damping function F_m

$$F_m = \begin{cases} \exp\left(-\frac{1}{4}\left[\frac{k}{k_m} - 1\right]^2\right) & \text{for } k > k_m \\ 1 & \text{for } k \leq k_m \end{cases} \quad (\text{A3})$$

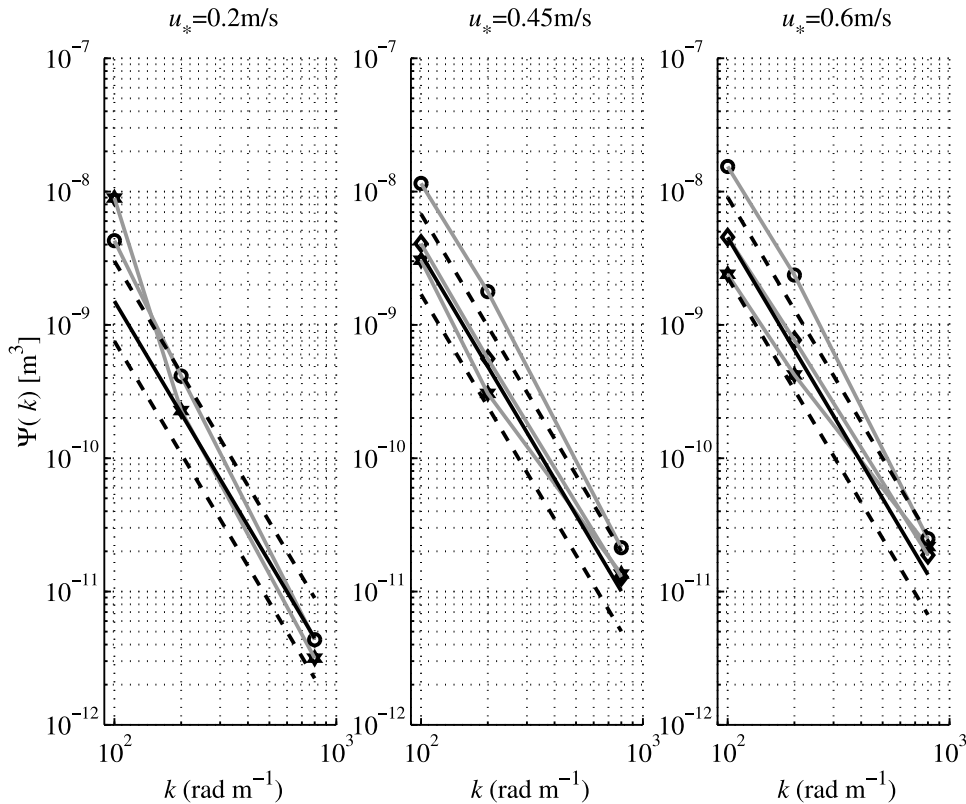


Figure A2. Comparison of high-wave number spectra for different u_* ; circles, Jähne and Riemer [1990] (100 m fetch); diamonds, Zhang [1995] (24 m fetch); stars, Hara *et al.* [1997] (13 m fetch); and solid line, parametric model (A2), with $m = 1$, $n = -2.8$, and 50% error in α (dashed lines).

where k_m is the wave number at minimum phase speed. Finally, the parameterized high-wave number spectrum is given by

$$\hat{\Psi}(k) = (\alpha \pm 0.5\alpha)F_m u_* k^{-2.8}. \quad (\text{A4})$$

[39] For a continuous omnidirectional spectrum, low- and high-wave number spectra are combined via a simple power law interpolation centered at $k = 200 \text{ rad m}^{-1}$. The choice of the wave number $k = 200 \text{ rad m}^{-1}$, which separates the low- and high-wave number spectra, can be justified as follows. Assume that the surface current penetrates to a depth l , so that waves with $k > 1/l$ are significantly advected by the surface current. The viscous sublayer reaches approximately a depth of $5\nu/u_{*vw} \approx 0.5 \text{ mm}$ (u_{*vw} is the viscous friction velocity in the water side). We further assume a linear subsurface current profile in the viscous sublayer and an aerodynamically smooth turbulent flow outside the viscous sublayer. For the reported surface current and viscous stress, the subsurface current is roughly 4 mm deep. Thus waves with about $k > 200 \text{ rad m}^{-1}$ should be significantly Doppler shifted. The directionality of the wave spectrum is described next.

A3. Directionality

[40] Donelan *et al.* [1985] showed that a hyperbolic secant distribution can describe accurately the directional spreading of gravity waves for laboratory and field measurements. The sech function is motivated by the analogy to soliton wave groups whose energy in the transverse direction of propagation is distributed like sech^2 . We modify Donelan *et al.*'s spreading function to allow a uniform spreading in the directions from $-\pi/2$ to $\pi/2$ relative to the wind for wave numbers that are greater than a wave number k_t

$$h_\Psi = \begin{cases} \text{sech}^2(b\theta)/\int_{-\pi/2}^{\pi/2} \text{sech}^2(b\theta) & \text{for } k \leq k_t \\ \frac{1}{\pi} & \text{for } k > k_t \end{cases} \quad (\text{A5})$$

Donelan's spreading function is defined such that $k_t \rightarrow \infty$, and $b = 1.24$ away from the peak. Note that the parameter b (Donelan *et al.*'s β) is a function of k , such that spreading is minimal close to the spectral peak. The uniform spreading component has been introduced because Zhang [1994] found that wind-forced gravity-capillary waves spread more uniformly such that b can be as small as $b \approx 0.8$. According to Zhang's study, mean b values are around 1.1, and display only a weak dependence on wind speed. In section 4 results are reported for a wave number spectrum with $b = 1.24$ for $k < 200 \text{ rad m}^{-1}$, $b = 1.1$ for $k > 200 \text{ rad m}^{-1}$, and $k_t \rightarrow \infty$ by default.

Appendix B: Contribution of Short Waves to Wave-Induced Stress

[41] To examine what fraction of the momentum flux is supported by shorter waves away from the frequently breaking dominant wave, we divide the wave spectrum into two parts, a low-wave number part that includes frequently breaking dominant waves and a remaining high-wave number part, with k_b as the dividing wave number. In four

experiments the breaking fraction of the dominant wave is larger than 85%, according to Banner and Peirson [1998, Table 1]. For simplicity, we will here only consider these four most extreme cases and we will assume that all waves with $k < k_b$ are breaking. First, we need to estimate k_b , i.e., the part of the spectrum that contains longer breaking waves.

[42] A rough approximation of the mean squared height of the dominant breaking wave follows from a breaking slope criterion. According to Banner and Peirson [1998], the mean wave slope is less than 0.3. Banner and Phillips [1974] showed that a surface drift, u_s , decreases Stokes' limiting wave slope by a factor of $(1 - u_s/c)^2$. To derive this result, Banner and Phillips assumed as the breaking criterion that the particle speed at the breaking wave crests exceeds the phase speed. Miller *et al.* [1999], however, showed that the particle speed at the breaking wave crest can be as small as half the phase speed, reducing the limiting wave slope even further (by as much as 60% of the value predicted by Banner and Phillips [1974]). With $u_s \approx 0.1 \text{ m/s}$, we estimate that the dominant waves likely break at a slope of $a_b k_p \sim 0.2$, where a_b is the breaking wave amplitude and k_p the wave number of the dominant wave (estimated by Banner and Peirson [1998]). Therefore k_b may be determined by

$$\frac{a_b^2}{2} = \frac{(0.2)^2}{2 k_p^2} = \int_0^{k_b} \int_{-\pi/2}^{\pi/2} \Psi k d\theta dk. \quad (\text{B1})$$

We find that k_b is close to the peak wave number with a maximal deviation from k_p of less than 35%. Shorter waves with $k > k_b$ contribute a significant fraction ranging from 50% to 95%, on average 65%, to the wave-induced momentum flux.

[43] **Acknowledgments.** We are grateful to William L. Peirson and Michael L. Banner for helpful comments, as well as for providing the wave height measurements. We would like to thank Stephen E. Belcher for stimulating discussions and two anonymous reviewers for constructive comments. This work was supported by the U.S. National Science Foundation (grant OCE0002314) and the U.S. Office of Naval Research (grant N00014-0110125).

References

- Banner, M. L. (1990), The influence of wave breaking on the surface pressure distribution in wind-wave interactions, *J. Fluid Mech.*, 211, 463–495.
- Banner, M. L., and W. L. Peirson (1998), Tangential stress beneath wind-driven air-water interfaces, *J. Fluid Mech.*, 364, 115–145.
- Banner, M. L., and O. M. Phillips (1974), On the incipient breaking of small scale waves, *J. Fluid Mech.*, 65, 647–656.
- Belcher, S. E. (1999), Wave growth by non-separated sheltering, *Eur. J. Mech. B*, 18, 447–462.
- Belcher, S. E., and J. C. R. Hunt (1993), Turbulent shear flow over slowly moving waves, *J. Fluid Mech.*, 251, 109–148.
- Belcher, S. E., and J. C. R. Hunt (1998), Turbulent flow over hills and waves, *Annu. Rev. Fluid Mech.*, 30, 507–538.
- Donelan, M. A., J. Hamilton, and W. H. Hui (1985), Directional spectra of wind-generated waves, *Philos. Trans. R. Soc. London, Ser. A*, 315, 509–562.
- Elfouhaily, T., B. Chapron, K. Katsaros, and D. Vandemark (1997), A unified directional spectrum for long and short wind-driven waves, *J. Geophys. Res.*, 102, 15,781–15,796.
- Hara, T., and S. E. Belcher (2002), Wind forcing in the equilibrium range of wind-wave spectra, *J. Fluid Mech.*, 470, 223–245.
- Hara, T., and S. E. Belcher (2004), Wind profile and drag coefficient over mature ocean surface wave spectra, *J. Phys. Oceanogr.*, 34, 2345–2358.

- Hara, T., E. J. Bock, and M. A. Donelan (1997), Frequency-wavenumber spectrum of wind-generated gravity-capillary waves, *J. Geophys. Res.*, *102*, 1067–1072.
- Harris, J. A., S. E. Belcher, and R. L. Street (1996), Linear dynamics of wind waves in coupled turbulent air-water flow. Part 2. Numerical model, *J. Fluid Mech.*, *308*, 219–254.
- Jähne, B. K., and K. S. Riemer (1990), Two-dimensional wave spectra of small water surface waves, *J. Geophys. Res.*, *95*, 11,531–11,546.
- Kawai, S. (1979), Generation of initial wavelets by instability of a coupled shear flow and their evolution to wind waves, *J. Fluid Mech.*, *93*, 661–703.
- Kudryavtsev, V. N., and V. K. Makin (2000), The impact of air-flow separation on the drag of the sea surface, *Boundary Layer Meteorol.*, *98*, 155–171.
- Kudryavtsev, V. N., V. K. Makin, and B. Chapron (1999), Coupled sea surface-atmosphere model: 2. Spectrum of short wind waves, *J. Geophys. Res.*, *104*, 7625–7640.
- Larson, T. R., and J. W. Wright (1975), Wind generated gravity-capillary waves: Laboratory measurements of temporal growth rates using micro-wave backscatter, *J. Fluid Mech.*, *70*, 417–436.
- Longuet-Higgins, M. S. (1963), The generation of capillary waves by steep gravity waves, *J. Fluid Mech.*, *16*, 138–159.
- Makin, V. K., and V. N. Kudryavtsev (1999), Coupled sea surface-atmosphere model: 1. Wind over waves coupling, *J. Geophys. Res.*, *104*, 7613–7623.
- Makin, V. K., V. N. Kudryavtsev, and C. Mastenbroek (1995), Drag of the sea surface, *Boundary Layer Meteorol.*, *73*, 159–182.
- Mastenbroek, C., V. K. Makin, M. H. Garat, and J. P. Giovanangeli (1996), Experimental evidence of the rapid distortion of turbulence in the air flow over water waves, *J. Fluid Mech.*, *318*, 273–302.
- Meirink, J. F., and V. K. Makin (2000), Modelling low-Reynolds-number effects in the turbulent air flow over water waves, *J. Fluid Mech.*, *415*, 155–174.
- Miles, J. W. (1962), On the generation of surface waves by shear flows. Part 4, *J. Fluid Mech.*, *13*, 433–448.
- Miller, M., T. Nennstiel, J. H. Duncan, A. A. Dimas, and S. Pröstler (1999), Incipient breaking of steady waves in the presence of surface wakes, *J. Fluid Mech.*, *383*, 285–305.
- Plant, W. J. (1982), A relationship between wind stress and wave slope, *J. Geophys. Res.*, *87*, 1961–1967.
- Plant, W. J., and J. W. Wright (1980), Phase speed of upwind and downwind traveling short gravity waves, *J. Geophys. Res.*, *85*, 3304–3310.
- Uz, B. M., M. A. Donelan, T. Hara, and E. J. Bock (2002), Laboratory studies of wind stress over surface wave, *Boundary Layer Meteorol.*, *102*, 301–331.
- Uz, B. M., T. Hara, E. J. Bock, and M. A. Donelan (2003), Laboratory observations of gravity-capillary waves under transient wind forcing, *J. Geophys. Res.*, *108*(C2), 3050, doi:10.1029/2000JC000643.
- van Gastel, K., P. A. E. M. Janssen, and G. J. Komen (1985), On phase velocity and growth rate of wind-induced gravity-capillary waves, *J. Fluid Mech.*, *161*, 199–216.
- Zhang, X. (1994), Wavenumber spectrum of very short wind waves: An application of two-dimensional Slepian windows to the spectral estimation, *J. Atmos. Oceanic Technol.*, *11*, 489–505.
- Zhang, X. (1995), Capillary-gravity and capillary waves generated in a wind wave tank: Observations and theories, *J. Fluid Mech.*, *289*, 51–82.

T. Hara and T. Kukulka, Graduate School of Oceanography, University of Rhode Island, Narragansett, RI 02882, USA. (tkukulka@gso.uri.edu)